Deep-Sea Research I 110 (2016) 90–98

Contents lists available at ScienceDirect

Deep-Sea Research I

journal homepage: www.elsevier.com/locate/dsri

Contrasting distributions of dissolved gaseous mercury concentration and evasion in the North Pacific Subarctic Gyre and the Subarctic Front

Hyunji Kim [a], Tae Siek Rhee [b], Doshik Hahm [b], Chung Yeon Hwang [b], Jisook Yang [a], Seunghee Han [a,*]

[a] School of Environmental Science and Engineering, Gwangju Institute of Science and Technology (GIST), Gwangju 500-712, Republic of Korea
[b] Korea Polar Research Institute, Incheon 406-840, Republic of Korea

ARTICLE INFO

Article history:
Received 1 October 2015
Received in revised form
25 January 2016
Accepted 2 February 2016
Available online 3 February 2016

Keywords:
Dissolved gaseous mercury
Chlorophyll-a
Apparent oxygen utilization
Subarctic Front
Subarctic Gyre
Dissolved organic matter

ABSTRACT

The distribution of dissolved gaseous mercury (DGM) and the oxidation–reduction processes of mercury (Hg) in the surface and subsurface ocean are currently understudied despite their importance in ocean–atmosphere interactions. We investigated the Hg(0) evasion and the DGM distribution at water depths of 2–500 m in the Subarctic Front, Western Subarctic Gyre, and Bering Sea of the Northwestern Pacific. The mean DGM concentration in the surface mixed water (<10 m) and the mean Hg(0) evasion flux were significantly higher in the Subarctic Front (125 ± 5.0 fM and 15 pmol m^{-2} h^{-1}, respectively), which typically has lower nutrient levels and higher primary production, than in the Western Subarctic Gyre and the Bering Sea (74 ± 18 fM and 3.2 ± 1.2 pmol m^{-2} h^{-1}, respectively). The variation in the chlorophyll-a concentration and extracellular protease activity predicted 54% and 48% of the DGM variation, respectively, in the euphotic zone (2–50 m). The DGM concentration in aphotic intermediate water (415 ± 286 fM) was positively correlated to the apparent oxygen utilization (AOU; $r^2=0.94$ and $p<0.001$ for the Western Subarctic Gyre and the Bering Sea; $r^2=0.61$ and $p=0.01$ for the Subarctic Front), emphasizing the importance of microbial oxidation of organic matter. The DGM-to-AOU ratio in aphotic water was significantly ($p<0.05$, ANCOVA) higher at the Western Subarctic Gyre and Bering Sea sites (2.5 ± 0.14) than the ratio at the Subarctic Front sites (0.89 ± 0.27) that mainly consisted of newly formed North Pacific Intermediate Water. The overall results imply that variation of DGM and Hg(0) evasion is closely linked to primary production in euphotic water and organic remineralization in aphotic intermediate water. The oceanic alterations in these factors may induce significant modification in Hg redox speciation in the Northwestern Pacific.

1. Introduction

Humans are exposed to mercury (Hg) mainly through consuming Hg-contaminated fish (Sunderland, 2007; Selin et al., 2010). Because most of the fish consumed by humans are of marine origin, understanding Hg speciation and cycling in the marine environment is a key issue related to human health risks. The surface and subsurface oceanic zones play essential roles in the biogeochemical cycling of Hg through a series of biotic and abiotic processes, as well as in fish production (Fitzgerald et al., 2007; Mason et al., 2012).

The removal of Hg(0) into the atmosphere through gas transfer is a key process in Hg ocean–atmosphere interactions (Costa and Liss, 1999, 2000). The ocean accounts for approximately 30–50% of the overall Hg flux into the atmosphere, and approximately 30–45% of Hg in the surface ocean is lost to atmospheric evasion through the reduced Hg pool (Soerensen et al., 2010; Mason et al., 2012). The distribution of Hg(0) and the oxidation–reduction processes of Hg in the surface and subsurface ocean are currently understudied despite their importance in ocean–atmosphere interactions (Fitzgerald et al., 2007; Mason et al., 2012).

Dissolved gaseous mercury (DGM) is operationally defined as a volatile Hg species that consists of elemental Hg, Hg(0), and dimethylmercury (DMHg; Kotnik et al., 2007). At the ocean surface, DGM is predominantly Hg(0) formed via Hg(II) reduction (Mason et al., 1995; Andersson et al., 2011). DGM production in surface seawater is dependent on light intensity and dissolved organic matter (DOM; Costa and Liss, 2000; Lanzillotta et al., 2002). The daily trends of DGM in Mediterranean coastal water matched the intensity of solar radiation, with higher levels of DGM found during maximum insolation (Lanzillotta et al., 2002). The role of

* Corresponding author.
E-mail address: shan@gist.ac.kr (S. Han).

http://dx.doi.org/10.1016/j.dsr.2016.02.001
0967-0637/

DOM in DGM production in surface seawater was shown during two oceanographic cruises in the Mediterranean basin (Fantozzi et al., 2007): the DGM concentration (0.05–0.10 pM) in offshore water was lower than that in coastal water (0.25–0.46 pM), which corresponds to the occurrence of lower concentrations of Hg(II) and DOM in offshore water. The limiting factors that affected DGM production in offshore water were the Hg(II) concentrations and a particular fraction of the DOM-absorbing light energy (Fantozzi et al., 2007). In contrast, %DGM/Hg increased in offshore water than in coastal water (Soerensen et al., 2013; Schartup et al., 2015). Increasing %DGM/Hg with a higher fraction of degraded terrestrial DOM, which was observed in Northwest Atlantic seawater, suggested that turnover of terrestrial DOM may increase the reduction rates of Hg–DOM complexes (Schartup et al., 2015). To date, however, the relationship between the quantity and quality of DOM and the DGM concentration in oceanic surface water is not clearly understood.

A steady increase in the DGM concentration in aphotic water with a decrease in the dissolved oxygen (DO) concentration was reported in the Mediterranean Sea and the Black Sea (Ferrara et al., 2003; Lamborg et al., 2008). These studies suggested that bacteria may produce DGM in suboxic seawater parallel to the photolytic reduction of Hg(II) that occurs at the ocean surface (Ferrara et al., 2003; Lamborg et al., 2008). The role of bacteria in DGM production under dark conditions was also suggested in a laboratory study in which no DGM production was present in sterilized coastal seawater samples (Fantozzi et al., 2009). DGM production was restored following reinoculation of the same water samples with a field-representative bacterial community (Fantozzi et al., 2009). Dissolved DMHg in the range of 5–20 fM was observed in the intermediate and deep waters of the North Pacific, which may contribute to the DGM concentration (Hammerschmidt and Bowman, 2012).

In the last few centuries, the global Hg concentration has continuously increased due to anthropogenic emissions, the largest sources of which have been artisanal gold mining and the combustion of fossil fuels (Pacyna et al., 2006, 2010). In 2005, Asia contributed approximately 67% of the global anthropogenic Hg emissions, and China, with more than 2000 coal-fired power plants, was the largest emitter in Asia (Pacyna et al., 2010). This situation raises concerns regarding the health of the marine ecosystem in the Northwestern Pacific (NWP). Global climate change also influences Hg bioaccumulation in marine ecosystems because climate change affects the transformation rates (e.g., methylation, demethylation, reduction, and oxidation) of Hg, as well as the composition of the biological community (Zheng and Kruse, 2006; Mueter and Litzow, 2008). The Bering Sea, a subarctic sea vulnerable to climate change, is one of the most suitable sites for monitoring the influence of climate change on the biogeochemical cycling of Hg and its impact on marine ecosystems (Piepenburg, 2005).

In the current study, we investigated the horizontal and vertical distributions of DGM at water depths of 2–500 m and the Hg (0) evasion from surface seawater at seven stations in the Subarctic Front, Western Subarctic Gyre, and Bering Sea in the NWP. To discuss the processes that explain DGM distribution and Hg (0) evasion in the NWP, spatial variances in DGM were compared to the phytoplankton biomass, extracellular protease activity, and apparent oxygen utilization. Because the Western Subarctic Gyre and the Bering Sea are high-nutrient, low-chlorophyll-a regions, in contrast to the Subarctic Front, we were able to assess the effects of distinct biological productivity on the DGM concentration and Hg(0) evasion flux.

2. Methods

2.1. Sampling and sample treatment

Seawater samples were collected from the upper 500 m of the NWP on board R/V Araon during the SHIPPO cruise from July 13 to 28, 2012 (Park and Rhee, 2015). Water samples for DGM analysis were collected in Teflon bottles, which were thoroughly acid-cleaned (30% v/v hydrochloric acid [HCl], at 70 °C for 24 h) and then filled with 1% (v/v) HCl while the bottles were stored. The Teflon bottles were thoroughly rinsed with sample water before they were filled using acid-cleaned silicon tubing (10% HCl at room temperature for 24 h).

Surface and subsurface seawater samples were collected at seven stations. At each station, the sampling depth was selected based on the temperature, salinity, DO, and photosynthetically active radiation, which were recorded in situ with a CTD-Rosette. Surface and deepwater samples were taken at 20- to 100-m water depth intervals using a Rosette sampler, on which 24 10-l Niskin bottles were mounted. The seawater samples used for the DGM analysis were collected from the Niskin bottles immediately after boarding without air disturbance in 2-l Teflon bottles to prevent the loss of volatile Hg.

2.2. DGM analysis

The DGM concentration in the seawater was determined on board immediately after sampling. First, 0.7- to 1.0-l water samples were transferred to an acid-cleaned glass bubbler (purging vessel) installed in a clean bench. The seawater sample was purged with Hg-free nitrogen gas (N_2) for 40 min with a flow rate of 300–400 ml min^{-1} (Mason et al., 2001). DGM was collected on a gold-coated bead trap. Elemental Hg was released by heating for 1 min in a flow of Hg-free N_2 and detected and quantified with a cold vapor atomic fluorescence spectrometer (Brooks Rand). The DGM collected with this method includes DMHg and Hg(0), as both species are volatile and can be collected on a gold trap.

A calibration curve was determined for each sample batch using a certified Hg(II) standard solution (10–200 pg) spiked in Milli-Q water. Here, Hg(II) was reduced to Hg(0) using a solution of stannous chloride prepared following EPA Method 1631. All DGM measurements were performed in duplicate, and the procedural precision averaged $11 \pm 10\%$ as a relative percentage difference ($n=104$). The measurement bias was determined at every ten samples using a Hg(II)-spiked Milli-Q solution, and was averaged to $104 \pm 6.9\%$ ($n=12$). The accuracy of the analysis was tested with the certified reference material (Institute for Reference Materials and Measurements, BCR-579). The Hg concentration in BCR-579 (Hg in coastal seawater) was determined after oxidation with a solution of bromine chloride followed by neutralization with $NH_2OH \cdot HCl$ (EPA Method 1631, 2000). The average recovery was $109 \pm 3.3\%$ ($n=8$). For matrix spike recovery, certified Hg(II) standard was spiked to the sample seawater due to lack of Hg (0) standard solution. Then Hg(0) concentration was measured after BrCl and $NH_2OH \cdot HCl$ treatment and stannous chloride reduction. The recovery of matrix spike averaged $103 \pm 16\%$ ($n=7$).

2.3. Nutrients and dissolved oxygen

The major nutrients (nitrate+nitrite, phosphate, silicate, and ammonium) were analyzed on board using a gas-segmented flow analysis system (QuAAtro, SEAL Analytical). Aliquots of seawater were subsampled into conical tubes from the Niskin water sampler, and the collected seawater samples were stored in a refrigerator until the analysis was conducted. The analytical system was calibrated with the KANSO reference material (Lot. No. 'BF,'

KANSO Technos) for nitrate+nitrite, phosphate, and silicate and with in-house standards for ammonium. To prevent contamination of the seawater samples by laboratory air, the auto-sampler was capped with a plastic film cover, into which fresh marine air from the foremast was pumped.

Preparation of the reagents and sampling of DO were performed using Knap et al.'s (1996) guidelines. Briefly, the water samples for DO were drawn first from the Niskin sampler and immediately pickled with the reagents. The sample bottles were stored in a cool, dark location, and the necks were sealed with water until the analysis was conducted. The DO concentrations were calculated by measuring the iodine concentration spectrophotometrically, as described by Labasque et al. (2004). The repeat measurements of the samples taken from the multiple Niskin bottles obtained at the same water depth suggested that the measurement precision was better than 0.3%. We calculated the apparent oxygen utilization (AOU) by subtracting the observed DO concentration from the saturated oxygen concentration at a given salinity and temperature. The saturated oxygen concentration was calculated using the equation described by Garcia and Gordon (1992).

2.4. Chlorophyll-a concentration, bacterial counts, and aminopeptidase activity

The chlorophyll-a concentration was measured fluorometrically using a Trilogy Laboratory Fluorometer (Turner Designs) according to a previously described method (Parsons et al., 1984). To measure bacterial abundance, the formalin-treated unfiltered seawater samples were filtered through 0.02 μm pore Anodisc filters (Whatman). The filters were immediately stained with 100 μl of diluted SYBR Gold (final dilution 2.5×10^3-fold) for 15 min in the dark (Noble and Fuhrman, 1998). The bacterial numbers were determined on board using an epifluorescence microscope (Olympus BX35).

Extracellular aminopeptidase activity was measured with the Hoppe method (1993), using a specific fluorogenic substrate (L-leucine-7-amido-4-methyl-coumarin, Leu-MCA) at a final concentration of 250 μM in triplicate 5 ml unfiltered samples. Increases in fluorescence were measured with a fluorometer (TBS-380, Turner Biosystems) immediately and after 3 h of incubation at the in situ temperature. A calibration curve of the Leu-MCA standard (Sigma) was performed in Milli-Q water at final concentrations of 0, 0.0025, 0.01, 0.05, and 0.2 μM.

2.5. Statistical analysis

Correlation and regression analyses were performed with SPSS 12.0 and SigmaPlot 12.0 software. A one-way analysis of variance (ANOVA) with a Tukey's test was used to assess significant differences in the DGM concentrations among the groups. The strength of the relationships between the DGM concentration and the geochemical parameters was analyzed with the Spearman correlation. A p value of less than 0.05 was considered statistically significant.

3. Results and discussion

3.1. Surface water circulation

The general circulation pattern of the sampling sites in the NWP is largely influenced by the Western Subarctic Gyre and the Bering Sea Gyre (Fig. 1; Harrison et al., 1999; Qiu, 2001; Yasuda, 2003). The East Kamchatka Current is a western boundary current of the Western Subarctic Gyre, which is formed by the mixing of outflow currents from the Bering Sea Gyre and the Alaskan Stream (Harrison et al., 1999, 2004). Part of the East Kamchatka Current enters the Sea of Okhotsk, where the current is modified along the Okhotsk Sea Gyre, which is a source of the North Pacific Intermediate Water (NPIW; Yasuda, 2003). The Okhotsk Sea water outflows back to the Pacific and combines with the East Kamchatka Current to form the Oyashio Current (Talley, 1991; Yasuda, 2003). Part of the Oyashio Current recirculates northeastward

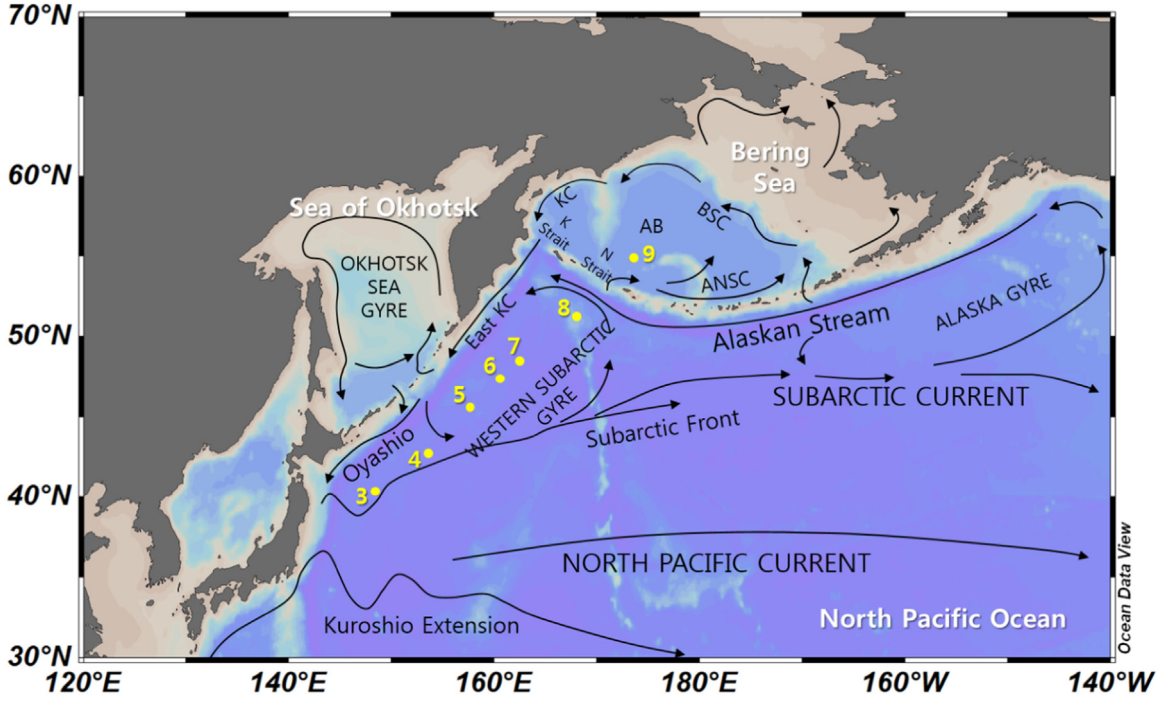

Fig. 1. Sampling locations (Sites 3–9) during the 2012 SHIPPO cruise and the surface currents in the Northwestern Pacific Ocean. BSC: Bering Slope Current; ANSC: Aleutian North Slope Current; KC: Kamchatka Current; N Strait: Near Strait; K Strait: Kamchatka Strait; and AB: Aleutian Basin.

along the Western Subarctic Gyre, whereas the other part flows southward and reaches the Kuroshio Extension (Yasuda, 2003).

The Alaskan Stream enters the Bering Sea (Site 9) from the eastern Pacific through many passes in the Aleutian Arc, including the Unimak Pass in the east and the Kamchatka Strait in the west (Fig. 1; Prants et al., 2013). Most of the flow into the Bering Sea occurs through the Near Strait, and this inflow is balanced by outflow through the Kamchatka Strait; thus, the circulation pattern of the Bering Sea is explained as a continuation of the Western Subarctic Gyre (Prants et al., 2013; Ladd, 2014).

3.2. Seawater properties

The surface salinity at Sites 3 and 4 was distinctively higher and the DO distinctively lower than at the other sites, reflecting the mixing effect of saline and old Kuroshio water (Fig. S1, Supporting information). The zone between the Kuroshio Extension and the Subarctic Front is referred to as the Kuroshio–Oyashio interfrontal zone, where intense meso-scale eddies are distributed due to the confluence of the subarctic and subtropical currents (Yasuda et al., 1996; Yasuda, 2003). The presence of the Subarctic Front is shown in the temperature–salinity (T–S) diagram in Fig. S1. In the 0–200 m layer (σ_θ 24.2–26.6), the water at Sites 3 and 4 had a higher saline concentration (salinity 33.3–33.6) than the water at Sites 5–9 (salinity 32.7–33.2). Sites 3 and 4 in the Subarctic Front have been reported to be the primary formation site of the new NPIW, defined as the salinity minimum in the subtropical North Pacific as an influence of Okhotsk Sea mode water (Talley, 1993; Shimizu et al., 2004). Once the NPIW is formed in the mixed-water region, just east of Hokkaido, subsequent modification along the NPIW's flow path increases the salinity and reduces the DO concentration (Talley, 1993; Reid, 1997; Shimizu et al., 2004).

3.3. DGM in surface water

The surface mixed water (< 10 m) DGM concentration in the NWP ranged from 53 to 132 fM, with an average concentration of 89 ± 28 fM (Figs. 2 and 3). This range is similar to the DGM range

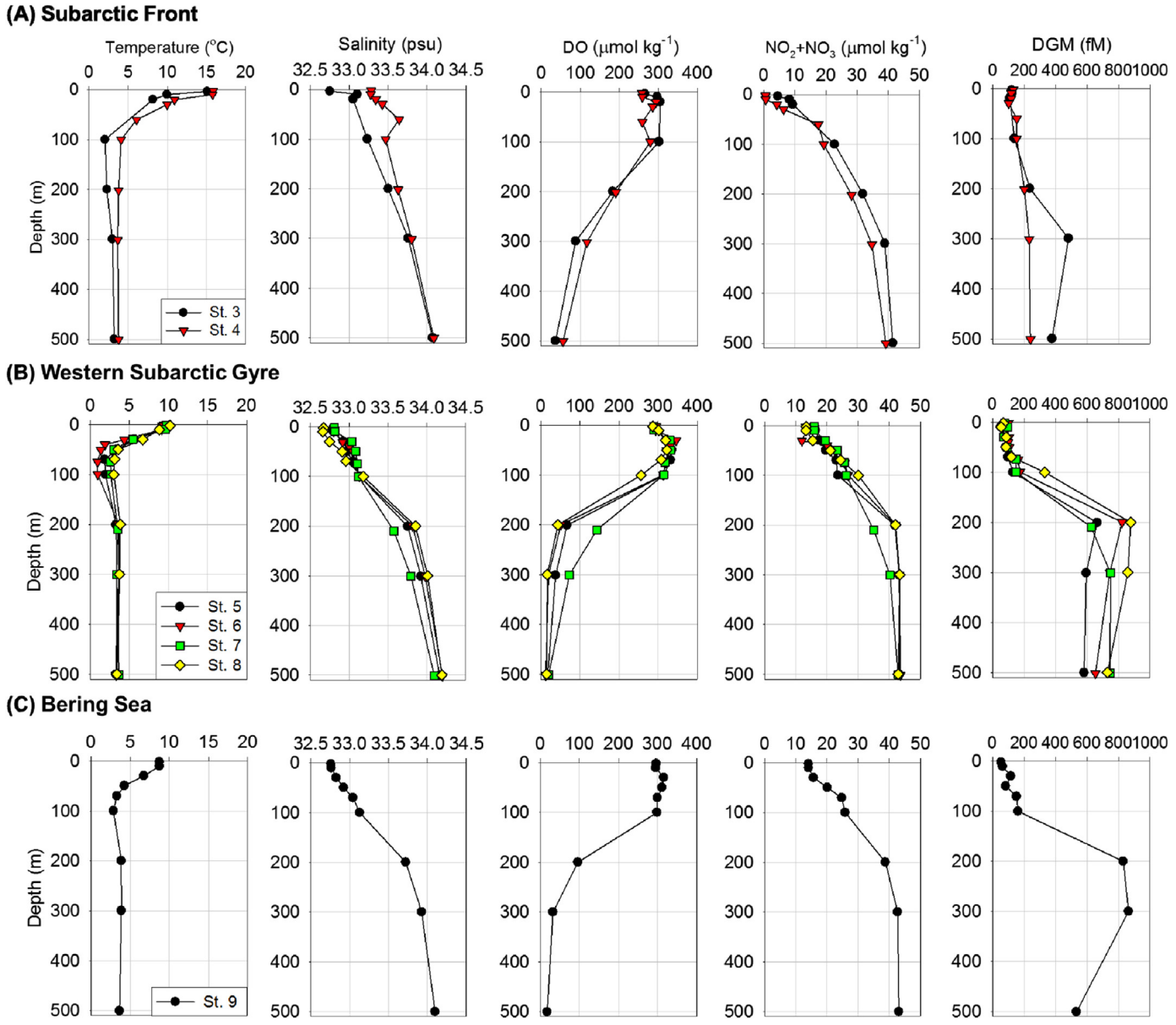

Fig. 2. Vertical distributions of temperature, salinity, dissolved oxygen (DO), nitrate+nitrite, and dissolved gaseous Hg (DGM) in the sampling locations of the Subarctic Front (Sites 3 and 4), Western Subarctic Gyre (Sites 5–8), and Bering Sea (Site 9).

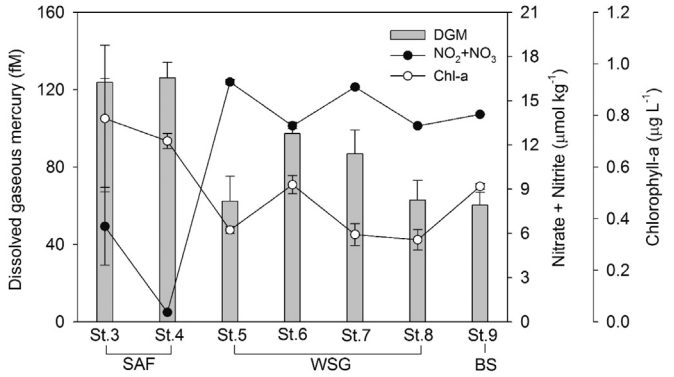

Fig. 3. Average concentrations (mean ± SD when $n > 3$) of dissolved gaseous mercury (DGM), nitrate+nitrite, and chlorophyll-a (Chl-a) found in the surface mixed layer (< 10 m) of the Subarctic Front (SAF, Sites 3 and 4), Western Subarctic Gyre (WSG, Sites 5–8), and Bering Sea (BS, Site 9).

determined in the tropical Pacific Ocean (47–105 fM; Soerensen et al., 2014), the North Atlantic Ocean (10–135 fM; Kuss et al., 2011; 150 ± 120 fM; Bowman et al., 2015), and the Baltic Sea (50–160 fM; Kuss and Schneider, 2007).

The DGM concentration in the surface mixed water was significantly ($p < 0.05$) lower in the Western Subarctic Gyre and the Bering Sea (74 ± 18 fM) than in the Subarctic Front (125 ± 5.0 fM; Fig. 3). In contrast, significantly ($p < 0.05$) higher nitrate+nitrite concentrations were observed at the surface of the Western Subarctic Gyre and the Bering Sea, which was reported as a high-nutrient, low-chlorophyll region, compared with the Subarctic Front (Harrison et al., 2004; Tyrrell et al., 2005; Aguilar-Islas et al., 2007). The low nutrient level of the Subarctic Front was attributed to the mixing with oligotrophic subtropical water (Tsurushima et al., 2002). The increasing pattern of chlorophyll-a concentration from north to south along the subarctic NWP was previously observed (Midorikawa et al., 2002).

Stepwise multiple regressions were performed using the Spearman correlation results to determine the independent variables for predicting the DGM concentration (Table 1). The multiple regression results showed that the most important predictor of DGM in the euphotic zone was the chlorophyll-a concentration. The faster Hg(II) reduction rate and/or the slower Hg(0) oxidation rate in the Subarctic Front compared to the Western Subarctic Gyre and the Bering Sea could be ascribed to the phytoplankton biomass.

About 54% of the DGM variation in the euphotic zone was predicted by the chlorophyll-a concentration, as shown in Fig. 4A. This result suggests that biotic Hg(II) reduction could be a significant source of DGM in the euphotic water of the NWP. A link

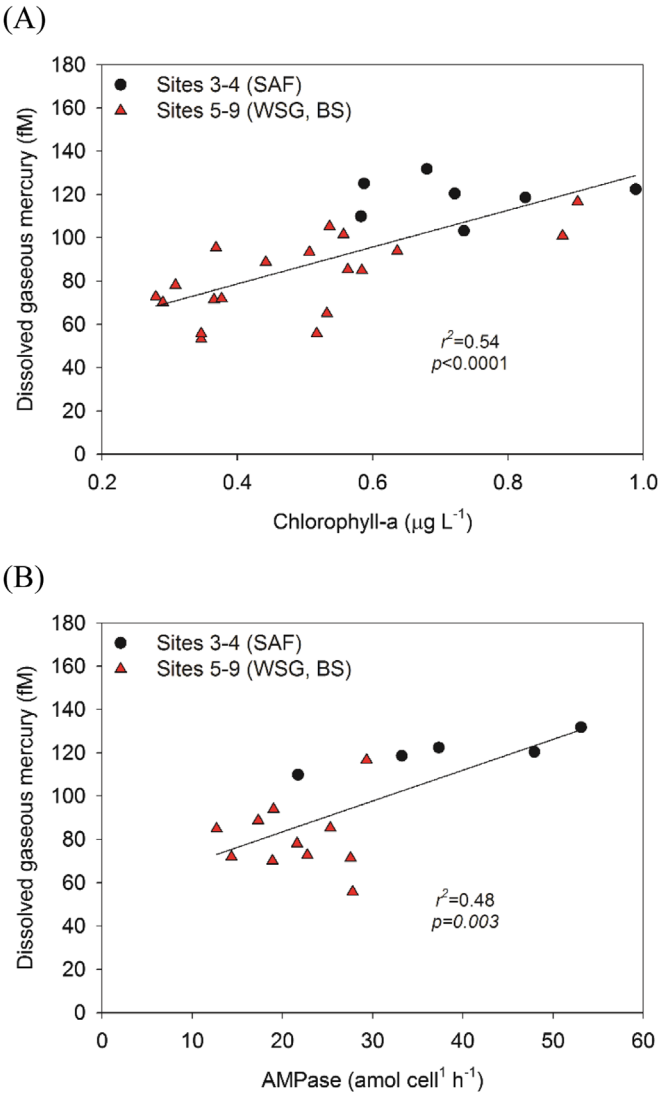

Fig. 4. Relationship between dissolved gaseous mercury and chlorophyll-a (A) and leucine aminopeptidase activity (AMPase) (B) in the euphotic zone (< 50 m) of the Subarctic Front (SAF, Sites 3 and 4), Western Subarctic Gyre (WSG, Sites 5–8), and Bering Sea (BS, Site 9). The lines indicate simple linear regression between dissolved gaseous mercury and chlorophyll-a ($y = 82x + 46$) and AMPase ($y = 1.4x + 55$). Aminopeptidase activity was measured from upper euphotic water only.

between primary production and the DGM concentration has been indicated previously: the global map of primary productivity closely matched the model approximation of global oceanic Hg

Table 1
The Spearman correlation coefficients for dissolved gaseous mercury (DGM) with temperature (Temp), density (Dens), salinity, dissolved oxygen (DO), apparent oxygen utilization (AOU), nitrate+nitrite (NO_2+NO_3), silicate (SiO_2), bacteria and viruses density, chlorophyll-a (chl-a), and aminopeptidase (AMPase) activity in the euphotic and aphotic waters of the sampling sites (Site 3–9). The stepwise multiple regression results are shown for the same sites. The number of data used in the Spearman correlation analysis is shown in parentheses. The chlorophyll-a concentration was measured from euphotic water only and aminopeptidase activity from upper euphotic water only.

	Temp	Dens	Salinity	DO	AOU	NO_2+NO_3	SiO_2	Bacteria	Viruses	Chl-a	AMPase
Euphotic (2–50 m)	0.34 (26)[a]	−0.32 (26)	0.62* (26)	−0.18 (26)	−0.31 (26)	−0.58** (26)	−0.56** (26)	−0.067 (26)	−0.38 (26)	0.78** (26)	0.57 (16)
	Stepwise multiple regression: [DGM] = 0.065[Chl-a] − 0.001[NO_2+NO_3] + 0.074, $R^2_{adj} = 0.75$, $p = 0.019$										
Aphotic (50–500 m)	0.47** (36)	0.76** (36)	0.78** (36)	−0.84** (36)	0.85** (36)	0.86** (36)	0.78** (36)	−0.57** (31)	−0.46** (31)	– –	– –
	Stepwise multiple regression: [DGM] = 0.026[NO_2+NO_3] − 0.47, $R^2_{adj} = 0.79$, $p < 0.001$										

* Statistical significance of $p < 0.05$.
** Statistical significance of $p < 0.01$.

Table 2
Summarized results from the DGM evasion flux calculation. Positive sign indicates sea-to-air flux.

Sampling site	Location	DGM seawater (pmol m^{-3})	Hg(0) air (pmol m^{-3})	Surface temperature (°C)	Wind speed (m s^{-1})	Hg(0) transfer velocity (m h^{-1})[a]	Henry's constant[b]	Flux (pmol m^{-2} h^{-1})
3	Subarctic Front	122	7.7	13	11	0.23	0.24	21
4		132	8.6	16	6.7	0.092	0.23	8.8
5	Western Subarctic Gyre	71	8.7	9.2	9.9	0.16	0.20	4.5
6		101	8.0	9.2	6.0	0.065	0.20	4.0
7		78	8.3	10	7.5	0.10	0.20	3.7
8		70	8.0	10	5.8	0.062	0.20	1.9
9	Bering Sea	56	8.3	8.8	8.9	0.13	0.20	1.8

[a] Calculated with equation $k=(0.22u^2+0.333u)\times(Sc_{Hg}/600)^{-0.5}$ according to Nightingale et al. (2000), where u is wind speed and Sc_{Hg} is the Schmidt number of Hg(0).
[b] Calculated with equation $H=e^{-2404.3/T+6.92}$ according to Andersson et al. (2008), where T is the seawater temperature (K).

evasion, showing higher evasion in the productive region (North Atlantic, 300 pmol m^{-2} day^{-2}) and lower evasion in the oligotrophic region (North Pacific, 30 pmol m^{-2} day^{-2}; Mason et al., 1994). Mason et al. (1995) reported that eukaryotic phytoplankton are capable of reducing Hg(II), based on the observation of a strong correlation between Hg(0) and chlorophyll-a. The significant contribution of cellular density to %DGM/Hg, measured in a culture of *Thalassiosira weissflogii*, was observed under light and dark conditions (Morelli et al., 2009).

The DGM production mechanism associated with phytoplankton biomass might be that biogenic substances are released from phytoplankton, and these substances enhance Hg(II) reduction rates, as cell exudates of marine diatom have increased DGM production under light and dark conditions (Lanzillotta et al., 2004). In the same report, a higher photo-production rate (2.2 ± 0.02 pg min^{-1} l^{-1}) compared to the control medium (0.56 ± 0.16 pg min^{-1} l^{-1}) was determined from the artificial seawater amended with filtered cell exudates of the marine diatom *Chaetoceros* (Lanzillotta et al., 2004).

The importance of cell exudates or DOM for increased DGM production is supported by the fact that higher DGM concentrations were found at the surface of Sites 3 and 4 where relatively higher leucine aminopeptidase activities, which has been shown to represent bacterial metabolic processes involved in protein degradation (Martinez and Azam, 1993; Caruso and Zaccone, 2000), were found (Fig. 4B). The leucine aminopeptidase activity in euphotic water was 39 ± 12 amol $cell^{-1}$ h^{-1} at Sites 3 and 4 and 22 ± 5.6 amol $cell^{-1}$ h^{-1} at Sites 5–9 (Fig. 4B). About 48% of the DGM variation in the euphotic zone was predicted by leucine aminopeptidase activity ($p=0.003$), suggesting that the increased DGM concentration at Sites 3 and 4 may be associated with enhanced DOM availability (Schartup et al., 2015). A similar implication was suggested in a study of Long Island coastal water: the Hg(II) reduction rates in light/dark incubation as well as the bacterial counts were observed to be higher during the late spring when the chlorophyll-a concentration and microbial activity were higher than during the summer and fall (Rolfhus and Fitzgerald, 2004).

The higher DGM concentration in the Subarctic Front could be partly ascribed to the low nitrate+nitrite concentrations based on the stepwise multiple regression results showing a negative correlation between nitrate+nitrite and DGM for euphotic water (Table 1). Nitrite is known to function as an oxidant precursor by releasing hydroxyl radicals upon photolysis (Mason et al., 2001). In the presence of 100 and 1000 μM of nitrite in seawater, the DGM concentration decreased from 0.7 to 0.2 pM after 30 min of incubation of seawater under a broadband light (Mason et al., 2001). However, the same result has not been confirmed at natural levels (<10 μM) of nitrite.

3.4. Evasion of Hg(0)

The Hg(0) evasion flux (F) was estimated using Eq. (1), as most DGM is Hg(0) in surface seawater (Mason and Fitzgerald, 1991; Mason et al., 2001; Kotnik et al., 2007; Andersson et al., 2011).

$$F = k(C_w - C_a/H). \quad (1)$$

Here, C_w is the Hg(0) concentration in surface seawater (<3 m), C_a is the atmospheric Hg(0) concentration (*Rhee* et al., *Atmospheric Mercury Speciation Over the Northwestern Pacific, In Preparation*), and H is the dimensionless Henry's constant at the given seawater temperature (Andersson et al., 2008). The gas-transfer velocity of Hg(0), k, is calculated with Eq. (2) according to Nightingale et al. (2000):

$$k = (0.22u^2 + 0.333\,u) \times (Sc_{Hg}/600)^{-0.5}, \quad (2)$$

where u is the wind speed at each site, Sc_{Hg} is the Schmidt number of Hg(0) at the given seawater temperature (Kuss et al., 2009), and 600 is the Schmidt number of CO_2 at 20 °C. The estimation results are summarized in Table 2.

The estimated evasion flux ranged from 1.8 to 21 pmol m^{-2} h^{-1}, with an average flux of 6.5 ± 6.7 pmol m^{-2} h^{-1} (Table 2). This range is similar to the evasion flux of the North Pacific found in the literature: 7.0 ± 1.0 pmol m^{-2} h^{-1} (14–20°N; wind speed, 9.8 ± 2.5 m s^{-1}; Hg(0), 1.3 ± 0.05 ng m^{-3}; DGM, 51 ± 4.1 fM; Soerensen et al., 2014). The corresponding $t_{1/2}$ of DGM was estimated to be 8.7–47 h, suggesting that in situ Hg(II) reduction is required to support the steady-state DGM concentration in the surface mixed layer.

Significantly ($p<0.05$) higher evasion flux was determined for the Subarctic Front (21 and 8.8 pmol m^{-2} h^{-1}) than for the Western Subarctic Gyre and the Bering Sea (1.8–4.5 pmol m^{-2} h^{-1}), along with an increasing trend from north to south (Fig. 5). The higher evasion at the Subarctic Front was influenced by the higher DGM concentration, and in turn, the higher DGM concentration was associated with large phytoplankton biomass and proteolytic enzyme activity, as shown in Fig. 4. In fact, the Hg(0) evasions at the Subarctic Front are in agreement with those found from the productive oceanic zone (e.g., North Atlantic, 300 pmol m^{-2} day^{-2}). These results suggest that biological productivity is closely associated with the evasion of Hg(0) (Mason et al., 1994, 1995).

3.5. DGM in intermediate water

The DGM concentration increased as the depth increased in the

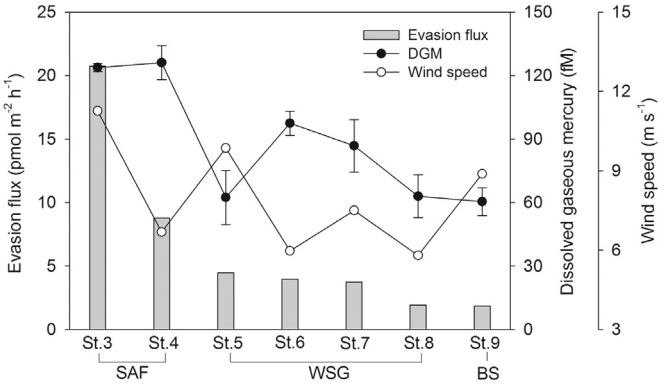

Fig. 5. Evasion flux of Hg(0), wind speed, and dissolved gaseous mercury (DGM) concentration in surface water in the sampling locations of the Subarctic Front (SAF, Sites 3 and 4), Western Subarctic Gyre (WSG, Sites 5–8), and Bering Sea (BS, Site 9).

oxycline of 100–200 m or 100–300 m and then remained constant or decreased until 500 m, with the exception at Site 4 (Fig. 2). Site 4 in the Subarctic Front showed more or less constant distribution by depth. The nitrate+nitrite concentration showed a similar vertical pattern to the DGM concentration except for the steady increase by depth observed at Site 4. DGM in suboxic water may include a significant amount of DMHg (Kotnik et al., 2007). The DMHg-to-DGM ratio was estimated to be <0.26 in the surface oxic layer (0–100 m; DO, 250–350 μmol kg^{-1}), whereas the ratio increased to 0.27–0.35 in the intermediate layer (100–300 m; DO, 20–300 μmol kg^{-1}) in the Northeastern Pacific (Hammerschmidt and Bowman, 2012).

The DGM distribution in aphotic intermediate water increased with increases in the AOU and the nitrate+nitrite concentration (Fig. 6). The 94% of the DGM variation, excluding the 500-m data, was explained by the AOU at Sites 5–9. Similarly, the 93% DGM variation was explained by the nitrate+nitrite variation at Sites 5–9 without the 500-m data. The remineralization of sinking organic matter by microorganisms may play a critical role in the production of DGM (Ferrara et al., 2003; Horvat et al., 2003).

The lower intermediate water found at a water depth of 500 m (σ_θ 27.0–27.2) at Sites 5 to 9 showed a lower DGM-to-AOU ratio than the ratio of the upper water (Fig. 6). The low organic carbon remineralization rate, expected from lower intermediate water, may explain the low DGM-to-AOU ratio. The lower intermediate waters of the Western Subarctic Gyre and the Bering Sea include a component that originated in the Pacific Deep Water (Laurier et al., 2004; Firdaus et al., 2008). Watanabe et al. (1991) estimated the formation years of the isopycnal horizons (σ_θ 26.6–27.4) of the Western Subarctic Gyre using tritium concentrations found in the Western Subarctic Gyre and the end-member waters (i.e., the Okhotsk Sea and the Bering Sea). The results showed that the Western Subarctic Gyre water was from 0 to 15 years old for σ_θ 26.6–27.0 (200–450 m) and from 15 to 22 years old for σ_θ 27.0–27.2 (approximately 500 m) water depth (Watanabe et al., 1991).

The DGM-to-AOU ratio was lower in the intermediate depth of the Subarctic Front than in the Western Subarctic Gyre and the Bering Sea (Sites 5–9). The new NPIW, characterized by low salinity (as low as 33.8) and high DO, is found at a water depth of 50–500 m of the Subarctic Front (Talley, 1993; Reid, 1997; Bostock et al., 2010). The new NPIW is known to be formed in the Kuroshio–Oyashio interfrontal zone via the mixing of different waters, i.e., Okhotsk Sea water, Japan/East Sea water, and the existing NPIW (You, 2003; Bostock et al., 2010). The formation of the new NPIW in the subsurface justifies no separation of the DGM-to-AOU ratio at the 500-m water depth that was shown for the northern sites (the Western Subarctic and the Bering Sea). The organic carbon remineralization rate averaged 5.3 ± 1.3 for the North

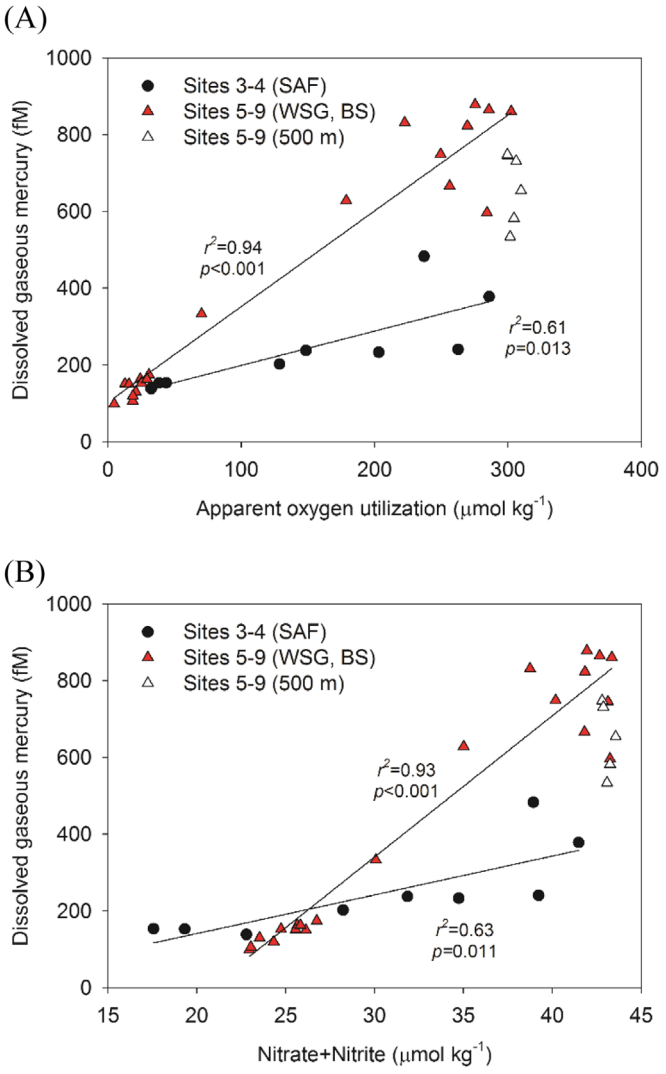

Fig. 6. Relationship between dissolved gaseous mercury and (A) apparent oxygen utilization and (B) nitrate+nitrite concentration found in 50 to 500 m of the Subarctic Front (SAF, Sites 3 and 4), Western Subarctic Gyre (WSG, Sites 5–8), and Bering Sea (BS, Site 9). The lines indicate a simple linear regression model: (A) $y=0.89x+110$ for Sites 3 and 4 and $y=2.5x+103$ for Sites 5–9 excluding 500 m water depth; (B) $y=10x-60$ for Sites 3 and 4 and $y=37x-763$ for Sites 5–9 excluding 500 m water depth.

Pacific subarctic water and 3.8 ± 1.7 μmol kg^{-1} yr^{-1} for the NPIW (Sunderland et al., 2009). A lower organic carbon remineralization rate could be part of the reason for the lower DGM-to-AOU ratio in the Subarctic Front.

4. Conclusions

The DGM concentrations in surface and subsurface waters were measured in two contrasting areas of the Subarctic Front and the Subarctic Gyre in the NWP. The biological productivity in the Subarctic Gyre is typically lower than the Subarctic Front, as known as a high-nutrient, low-chlorophyll region. In surface mixed water, the average DGM concentration measured in the Subarctic Front was 125 ± 5.0 fM, ranging from 120 to 132 fM. The DGM concentrations observed in the Subarctic Front were 1.6 times the concentrations measured in the Subarctic Gyre (77 ± 18 fM), ranging from 53 to 101 fM, suggesting a possible linkage between DGM concentration and biological productivity. The higher DGM concentrations in the Subarctic Front resulted in

the higher Hg(0) evasion (15 pmol m^{-2} h^{-1}) in the Subarctic Front than in the Subarctic Gyre (3.2 ± 1.2 pmol m^{-2} h^{-1}). On the contrary, in aphotic water, enhanced DGM concentrations were measured at the Subarctic Gyre than the Subarctic Front, indicating that DGM formation is relatively low in the newly formed NPIW. Overall results emphasize the dynamic nature of the DGM production in the NWP largely influenced by biological productivity.

The duration and extent of seasonal sea ice and seawater temperature are critical controls for primary production and microbial activity in the NWP (Grebmeier et al., 2006). Numerous studies have recently reported that in the NWP sea ice is gradually retreating northward and the water column is warming (Moore et al., 2006; Mueter and Litzow, 2008). The hydrographic changes related to the extent of seasonal sea ice in the Bering Sea and the consequent shift of the Subarctic Front in the NWP are likely to affect the Hg(0) evasion via control of primary production and associated microbial activity. Impact of Subarctic Front shift in the NWP on the redox process of Hg should therefore be further investigated.

Acknowledgments

This work was supported by the Korea Polar Research Institute (KOPRI) via the Korean Polar Research Program (SHIPPO, PE13410 and PM15070), the National Research Foundation (NRF-2015R1A2AA01003774), and the Ministry of Oceans and Fisheries (Long-term Change of Structure and Function in Marine Ecosystems of Korea-20140507).

Appendix A. Supplementary material

Supplementary data associated with this article can be found in the online version at http://dx.doi.org/10.1016/j.dsr.2016.02.001.

References

Aguilar-Islas, A.M., Hurst, M.P., Buck, K.N., Sohst, B., Smith, G.J., Lohan, M.C., Bruland, K.W., 2007. Micro-and macronutrients in the southeastern Bering Sea: insight into iron-replete and iron-depleted regimes. Prog. Oceanogr. 73 (**2**), 99–126. http://dx.doi.org/10.1016/j.pocean.2006.12.002.

Andersson, M.E., Gårdfeldt, K., Wängberg, I., Strömberg, D., 2008. Determination of Henry's law constant for elemental mercury. Chemosphere 73, 587–592. http://dx.doi.org/10.1016/j.chemosphere.2008.05.067.

Andersson, M.E., Sommar, J., Gårdfeldt, K., Jutterström, S., 2011. Air-sea exchange of volatile mercury in the North Atlantic Ocean. Mar. Chem. 125 (1–4), 1–7. http://dx.doi.org/10.1016/j.marchem.2011.01.005.

Bostock, H.C., Opdyke, B.N., Williams, M.J., 2010. Characterising the intermediate depth waters of the Pacific Ocean using $\delta^{13}C$ and other geochemical tracers. Deep Sea Res. Part I 57 (**7**), 847–859. http://dx.doi.org/10.1016/j.dsr.2010.04.005.

Bowman, K.L., Hammerschmidt, C.R., Lamborg, C.H., Swarr, G., 2015. Mercury in the North Atlantic Ocean: the US GEOTRACES zonal and meridional sections. Deep Sea Res. Part II 116, 251–261. http://dx.doi.org/10.1016/j.dsr2.2014.07.004.

Caruso, G., Zaccone, R., 2000. Estimates of leucine aminopeptidase activity in different marine and brackish environments. J. Appl. Microbiol. 89 (6), 951–959. http://dx.doi.org/10.1046/j.1365-2672.2000.01198.x.

Costa, M., Liss, P., 1999. Photoreduction of mercury in sea water and its possible implications for Hg0 air-sea fluxes. Mar. Chem. 68 (1–2), 87–95. http://dx.doi.org/10.1016/S0304-4203(99)00067-5.

Costa, M., Liss, P., 2000. Photoreduction and evolution of mercury from seawater. Sci. Total Environ. 261 (1–3), 125–135. http://dx.doi.org/10.1016/S0048-9697(00)00631-8.

EPA Method 1631, 2000. Revision E: Mercury in Water by Oxidation, Purge and Trap, and Cold Vapor Atomic Fluorescence Spectrometry. United States Environmental Protection Agency, Washington, DC.

Fantozzi, L., Ferrara, R., Frontini, F., Dini, F., 2007. Factors influencing the daily behaviour of dissolved gaseous mercury concentration in the Mediterranean Sea. Mar. Chem. 107, 4–12. http://dx.doi.org/10.1016/j.marchem.2007.02.008.

Fantozzi, L., Ferrara, R., Frontini, F., Dini, F., 2009. Dissolved gaseous mercury production in the dark: Evidence for the fundamental role of bacteria in different types of Mediterranean water bodies. Sci. Total Environ. 407 (2), 917–924. http://dx.doi.org/10.1016/j.scitotenv.2008.09.014.

Ferrara, R., Ceccarini, C., Lanzillotta, E., Gårdfeldt, K., Sommar, J., Horvat, M., Logar, M., Fajon, V., Kotnik, J., 2003. Profiles of dissolved gaseous mercury concentration in the Mediterranean seawater. Atmos. Environ. 37 (Suppl. 1), S85–S92. http://dx.doi.org/10.1016/S1352-2310(03)00248-6.

Firdaus, M.L., Norisuye, K., Nakagawa, Y., Nakatsuka, S., Sohrin, Y., 2008. Dissolved and labile particulate Zr, Hf, Nb, Ta, Mo and W in the western North Pacific Ocean. J. Oceanogr. 64 (2), 247–257. http://dx.doi.org/10.1007/s10872-008-0019-z.

Fitzgerald, W.F., Lamborg, C.H., Hammerschmidt, C.R., 2007. Marine biogeochemical cycling of mercury. Chem. Rev. 107 (2), 641–662. http://dx.doi.org/10.1021/cr050353m.

Garcia, H.E., Gordon, L.I., 1992. Oxygen solubility in seawater: better fitting equations. Limnol. Oceanogr. 37 (6), 1307–1312. http://dx.doi.org/10.4319/lo.1992.37.6.1307.

Grebmeier, J.M., Cooper, L.W., Feder, H.M., Sirenko, B.I., 2006. Ecosystem dynamics of the Pacific-influenced northern Bering and Chukchi Seas in the Amerasian Arctic. Prog. Oceanogr. 71 (2), 331–361. http://dx.doi.org/10.1126/science.1121365.

Hammerschmidt, C.R., Bowman, K.L., 2012. Vertical methylmercury distribution in the subtropical North Pacific Ocean. Mar. Chem. 132–133, 77–82. http://dx.doi.org/10.1016/j.marchem.2012.02.005.

Harrison, P.J., Boyd, P.W., Varela, D.E., Takeda, S., Shiomoto, A., Odate, T., 1999. Comparison of factors controlling phytoplankton productivity in the NE and NW subarctic Pacific gyres. Prog. Oceanogr. 43 (2–4), 205–234. http://dx.doi.org/10.1016/S0079-6611(99)00015-4.

Harrison, P.J., Whitney, F.A., Tsuda, A., Saito, H., Tadokoro, K., 2004. Nutrient and plankton dynamics in the NE and NW gyres of the subarctic Pacific Ocean. J. Oceanogr. 60 (1), 93–117. http://dx.doi.org/10.1023/B:JOCE.0000038321.57391.2a.

Hoppe, H.G., 1993. Use of fluorogenic model substrates for extracellular enzyme activity (EEA) measurement of bacteria. In: Kemp, P.F., Sherr, B.F., Sherr, E.B., Cole, J.J. (Eds.), Handbook of Methods in Aquatic Microbial Ecology, pp. 423–431.

Horvat, M., Kotnik, J., Logar, M., Fajon, V., Zvonarić, T., Pirrone, N., 2003. Speciation of mercury in surface and deep-sea waters in the Mediterranean Sea. Atmos. Environ. 37 (Supplement No.1), S93–S108. http://dx.doi.org/10.1016/S1352-2310(03)00249-8.

Knap A., Michaels A., Close A., Ducklow H., Dickson A., 1996. Protocols for the joint global ocean flux study (JGOFS) core measurements. JGOFS, Reprint of the IOC Manuals and Guides No. 29, UNESCO, p. 19.

Kotnik, J., Horvat, M., Tessier, E., Ogrinc, N., Monperrus, M., Amouroux, D., Fajon, V., Gibičar, D., Žižek, S., Sprovieri, F., Pirrone, N., 2007. Mercury speciation in surface and deep waters of the Mediterranean Sea. Mar. Chem. 107 (1), 13–30. http://dx.doi.org/10.1016/j.marchem.2007.02.012.

Kuss, J., Schneider, B., 2007. Variability of the gaseous elemental mercury sea–air flux of the Baltic Sea. Environ. Sci. Technol. 41, 8018–8023. http://dx.doi.org/10.1021/es0716251.

Kuss, J., Holzmann, J., Ludwig, R., 2009. An elemental mercury diffusion coefficient for natural waters determined by molecular dynamics simulation. Environ. Sci. Technol. 43 (9), 3183–3186. http://dx.doi.org/10.1021/es8034889.

Kuss, J., Zülicke, C., Pohl, C., Schneider, B., 2011. Atlantic mercury emission determined from continuous analysis of the elemental mercury sea-air concentration difference within transects between 50°N and 50°S. Global Biogeochem. Cycles 25, GB3021. http://dx.doi.org/10.1029/2010GB003998.

Labasque, T., Chaumery, C., Aminot, A., Kergoat, G., 2004. Spectrophotometric Winkler determination of dissolved oxygen: re-examination of critical factors and reliability. Mar. Chem. 88 (1), 53–60. http://dx.doi.org/10.1016/j.marchem.2004.03.004.

Ladd, C., 2014. Seasonal and interannual variability of the Bering Slope Current. Deep Sea Res. Part II 109, 5–13. http://dx.doi.org/10.1016/j.dsr2.2013.12.005.

Lamborg, C.H., Yiğiterhan, O., Fitzgerald, W.F., Balcom, P.H., Hammerschmidt, C.R., Murray, J., 2008. Vertical distribution of mercury species at two sites in the Western Black Sea. Mar. Chem. 111 (1–2), 77–89. http://dx.doi.org/10.1016/j.marchem.2007.01.011.

Lanzillotta, E., Ceccarini, C., Ferrara, R., Dini, F., Frontini, F.P., Banchetti, R., 2004. Importance of the biogenic organic matter in photo-formation of dissolved gaseous mercury in a culture of the marine diatom Chaetoceros sp. Sci. Total Environ. 318, 211–221. http://dx.doi.org/10.1016/S0048-9697(03)00400-5.

Lanzillotta, E., Ceccarini, C., Ferrara, R., 2002. Photo-induced formation of dissolved gaseous mercury in coastal and offshore seawater of the Mediterranean basin. Sci. Total Environ. 300, 179–187. http://dx.doi.org/10.1016/S0048-9697(02)00223-1.

Laurier, F., Mason, R., Gill, G.A., Whalin, L., 2004. Mercury distributions in the North Pacific Ocean—20 years of observations. Mar. Chem. 90 (1), 3–19. http://dx.doi.org/10.1029/2003JD003625.

Martinez, J., Azam, F., 1993. Aminopeptidase activity in marine chroococcoid cyanobacteria. Appl. Environ. Microbiol. 59 (11), 3701–3707.

Mason, R.P., Choi, A.L., Fitzgerald, W.F., Hammerschmidt, C.R., Lamborg, C.H., Soerensen, A.L., Sunderland, E.M., 2012. Mercury biogeochemical cycling in the ocean and policy implications. Environ. Res. 119, 101–117. http://dx.doi.org/10.1016/j.envres.2012.03.013.

Mason, R.P., Fitzgerald, W.F., 1991. Mercury speciation in open ocean. Water Air Soil Pollut. 56 (1), 779–789. http://dx.doi.org/10.1007/BF00342316.

Mason, R.P., Fitzgerald, W.F., Morel, F.M., 1994. The biogeochemical cycling of elemental mercury: anthropogenic influences. Geochim. Cosmochim. Acta 58 (15), 3191–3198. http://dx.doi.org/10.1016/0016-7037(94)90046-9.
Mason, R.P., Lawson, N.A., Sheu, G.-R., 2001. Mercury in the Atlantic Ocean: factors controlling air–sea exchange of mercury and its distribution in the upper waters. Deep Sea Res. Part II 48 (13), 2829–2853. http://dx.doi.org/10.1016/S0967-0645(01)00020-0.
Mason, R.P., Rolfhus, K.R., Fitzgerald, W.F., 1995. Methylated and elemental mercury cycling in surface and deep ocean waters of the North Atlantic. Water Air Soil Pollut. 80 (1–4), 665–677. http://dx.doi.org/10.1007/BF01189719.
Midorikawa, T., Umeda, T., Hiraishi, N., Ogawa, K., Nemoto, K., Kubo, N., Ishii, M., 2002. Estimation of seasonal net community production and air–sea CO_2 flux basedon the carbon budget above the temperature minimum layer in the western subarctic North Pacific. Deep-Sea Res. 1 (49), 339–362. http://dx.doi.org/10.1016/S0967-0637(01)00054-1.
Moore, S.E., Stafford, K.M., Mellinger, D.K., Hildebrand, J.A., 2006. Listening for large whales in the offshore waters of Alaska. BioScience 56 (1), 49–55. http://dx.doi.org/10.1641/0006-3568(2006)056[0049:LFLWIT]2.0.CO;2.
Morelli, E., Ferrara, R., Bellini, B., Dini, F., Di Giuseppe, G., Fantozzi, L., 2009. Changes in the non-protein thiol pool and production of dissolved gaseous mercury in the marine diatom *Thalassiosira weissflogii* under mercury exposure. Sci. Total Environ. 408 (2), 286–293. http://dx.doi.org/10.1016/j.scitotenv.2009.09.047.
Mueter, F.J., Litzow, M.A., 2008. Sea ice retreat alters the biogeography of the Bering Sea continental shelf. Ecol. Appl. 18 (2), 309–320. http://dx.doi.org/10.1890/07-0564.1.
Nightingale, P.D., Malin, G., Law, C.S., Watson, A.J., Liss, P.S., Liddicoat, M.I., Boutin, J., Upstill-Goddard, R.C., 2000. In situ evaluation of air-sea gas exchange parameterizations using novel conservative and volatile tracers. Global Biogeochem. Cycles 14 (1), 373–387. http://dx.doi.org/10.1029/1999GB900091.
Noble, R.T., Fuhrman, J.A., 1998. Use of SYBR Green I for rapid epifluorescence counts of marine viruses and bacteria. Aquat. Microb. Ecol. 14 (2), 113–118. http://dx.doi.org/10.3354/ame014113.
Pacyna, J.M., Pacyna, E.G., Sundseth, K., Munthe, J., Wilson, S., Leaner, L., 2010. Global emission of mercury to the atmosphere from anthropogenic sources in 2005 and projections to 2020. Atmos. Environ. 44 (20), 2487–2499. http://dx.doi.org/10.1016/j.atmosenv.2009.06.009.
Pacyna, E.G., Pacyna, J.M., Steenhuisen, F., Wilson, S., 2006. Global anthropogenic mercury emission inventory for 2000. Atmos. Environ. 40 (22), 4048–4063. http://dx.doi.org/10.1016/j.atmosenv.2006.03.041.
Park, K., Rhee, T.S., 2015. Source characterization of carbon monoxide and oxone over the Northwestern Pacific in summer. Atmos. Environ. 111, 151–160. http://dx.doi.org/10.1016/j.atmosenv.2015.04.015.
Piepenburg, D., 2005. Recent research on Arctic benthos: common notions need to be revised. Polar Biol. 28 (10), 733–755. http://dx.doi.org/10.1007/s00300-005-0013-5.
Prants, S., Andreev, A., Budyansky, M., Uleysky, M.Y., 2013. Impact of mesoscale eddies on surface flow between the Pacific Ocean and the Bering Sea across the near strait. Ocean Model. 72, 143–152. http://dx.doi.org/10.1016/j.ocemod.2013.09.003.
Parsons, T.R., Maita, Y., Lalli, C.M., 1984. Manual of Chemical and Biological Methods for Seawater Analysis. Pergamon Press, United Kingdom.
Qiu, B., 2001. Kuroshio and Oyashio currents. Can. J. Fish. Aquat. Sci. 57 (178), 191. http://dx.doi.org/10.1006/rwos.2001.0350.
Reid, J.L., 1997. On the total geostrophic circulation of the Pacific Ocean: flow patterns, tracers, and transports. Prog. Oceanogr. 39 (4), 263–352. http://dx.doi.org/10.1016/S0079-6611(97)00012-8.
Rolfhus, K.R., Fitzgerald, W.F., 2004. Mechanisms and temporal variability of dissolved gaseous mercury production in coastal seawater. Mar. Chem. 90 (1), 125–136. http://dx.doi.org/10.1016/j.marchem.2004.03.012.
Schartup, A.T., Ndu, U., Balcom, P.H., Mason, R.P., Sunderland, E.M., 2015. Contrasting effects of marine and terrestrially derived dissolved organic matter on mercury speciation and bioavailability in seawater. Environ. Sci. Technol. 49 (10), 5965–5972. http://dx.doi.org/10.1021/es506274x.
Selin, N.E., Sunderland, E.M., Knightes, C.D., Mason, R.P., 2010. Sources of mercury exposure for U.S. seafood consumers: Implications for policy. Environ. Health Perspect. 118 (1), 137–143. http://dx.doi.org/10.1289/ehp.0900811.
Shimizu, Y., Iwao, T., Yasuda, I., Ito, S.-I., Watanabe, T., Uehara, K., Shikama, N., Nakano, T., 2004. Formation process of North Pacific Intermediate Water revealed by profiling floats set to drift on 26.7 σ_θ isopycnal surface. J. Oceanogr. 60 (2), 453–462. http://dx.doi.org/10.1023/B:JOCE.0000038061.55914.eb.
Soerensen, A.L., Sunderland, E.M., Holmes, C.D., Jacob, D.L., Yantosca, R.M., Skov, H., Christensen, J.H., Strode, S.A., Mason, R.P., 2010. An improved global model for air-sea exchange of mercury: high concentrations over the North Atlantic. Environ. Sci. Technol. **44**, 8574–8580. http://dx.doi.org/10.1021/es102032g.
Soerensen, A.L., Mason, R.P., Balcom, P.H., Sunderland, E.M., 2013. Drivers of surface ocean mercury concentrations and air–sea exchange in the West Atlantic Ocean. Environ. Sci. Technol. 47 (14), 7757–7765. http://dx.doi.org/10.1021/es401354q.
Soerensen, A.L., Mason, R.P., Balcom, P.H., Jacob, D.J., Zhang, Y., Kuss, J., Sunderland, E.M., 2014. Elemental mercury concentrations and fluxes in the tropical atmosphere and Ocean. Environ. Sci. Technol. 48, 11312–11319. http://dx.doi.org/10.1021/es503109p.
Sunderland, E.M., 2007. Mercury exposure from domestic and imported estuarine and marine fish in the U.S. seafood market. Environ. Health Perspect. 115 (2), 235–242. http://dx.doi.org/10.1289/ehp.9377.
Sunderland, E.M., Krabbenhoft, D.P., Moreau, J.W., Strode, S.A., Landing, W.M., 2009. Mercury sources, distribution, and bioavailability in the North Pacific Ocean: Insights from data and models. Global Biogeochem. Cycles 23 (2), GB2010. http://dx.doi.org/10.1029/2008GB003425.
Talley, L.D., 1991. An Okhotsk Sea water anomaly: Implications for ventilation in the North Pacific. Deep Sea Res. Part 1 (38), S171–S190. http://dx.doi.org/10.1016/S0198-0149(12)80009-4.
Talley, L.D., 1993. Distribution and formation of North Pacific intermediate water. J. Phys. Oceanogr. 23 (3), 517–537. http://dx.doi.org/10.1175/1520-0485(1993)023<0517:DAFONP>2.0.CO;2.
Tsurushima, N., Nojiri, Y., Imai, K., Watanabe, S., 2002. Seasonal variations of carbon dioxide system and nutrients in the surface mixed layer at station KNOT (44°N, 155°E) in the subarctic western North Pacific. Deep-Sea Res. Part II 49, 5377–5394. http://dx.doi.org/10.1016/S0967-0645(02)00197-2.
Tyrrell, T., Merico, A., Waniek, J., Wong, C., Metzl, N., Whitney, F., 2005. Effect of seafloor depth on phytoplankton blooms in high-nitrate, lowchlorophyll (HNLC) regions. J. Geophys. Res. 110, G02007. http://dx.doi.org/10.1029/2005JG000041.
Watanabe, Y.W., Watanabe, S., Tsunogai, S., 1991. Tritium in the northwestern North Pacific. J. Oceanogr. Soc. Jpn. 47 (3), 80–93. http://dx.doi.org/10.1007/BF02301484.
Yasuda, I., 2003. Hydrographic structure and variability in the Kuroshio-Oyashio transition area. J. Oceanogr. 59 (4), 389–402. http://dx.doi.org/10.1023/A:1025580313836.
Yasuda, I., Okuda, K., Shimizu, Y., 1996. Distribution and modification of North Pacific intermediate water in the Kuroshio-Oyashio interfrontal zone. J. Phys. Oceanogr. 26 (4), 448–465. http://dx.doi.org/10.1175/1520-0485(1996)026<0448:DAMONP>2.0.CO;2.
You, Y., 2003. Implications of cabbeling on the formation and transformation mechanism of North Pacific Intermediate Water. J. Geophys. Res. 108 (C5). http://dx.doi.org/10.1029/2001JC001285.
Zheng, J., Kruse, G.H., 2006. Recruitment variation of eastern Bering Sea crabs: climate-forcing or top-down effects? Prog. Oceanogr. 68 (2–4), 184–204. http://dx.doi.org/10.1016/j.pocean.2006.02.002.